Mechanisms Determining Third Order Intermodulation Distortion in AlGaAs/GaAs Heterojunction Bipolar Transistors

Apostolos Samelis and Dimitris Pavlidis, *Senior Member, IEEE*

Abstract—**The third order intermodulation distortion (IMD3) mechanisms of HBT's are analyzed using Volterra Series theory. A T-equivalent circuit is used for the large-signal model of the HBT. The third order nonlinear currents generated by the device nonlinearities are evaluated for this purpose and current cancellation is discussed. It is found that, even though the C_{je} and g_{je} related currents do not show pronounced cancellation, the total base-emitter current and the total base-collector current cancel partially. Second harmonic loading is addressed in view of IMD3 optimization while, at the same time, maintaining high gain through conjugate matching at the fundamental frequency. IMD3 is very sensitive to the nonlinear currents generated by g_{je} and α. Optimum IMD3 occurs at high second harmonic reflection coefficients corresponding to open load conditions. Finally, minimum and maximum IMD3 occurs for second harmonic load reflection coefficient phases close to analogous extremes of the dominant nonlinear current of the device.**

I. Introduction

RECENT work on Heterojunction Bipolar Transistors (HBT's) demonstrated the merits of this device for low harmonic distortion applications as evidenced by their third order intermodulation characteristics [1]. Work on BJT amplifiers dating back to the 60's has shown that under certain bias or loading conditions third order product nullification may take place in the base-emitter junction. A more complete analysis on these aspects was reported by Narayanan [2] using Volterra Series.

Volterra Series has been extensively used for modeling frequency dependent distortion in weakly nonlinear devices [3]–[6]. Its implementation to bipolars (Si BJT's or HBT's) has been limited due to their inherently strong nonlinear behavior, which confines the dynamic range of calculations in the small signal region. This technique provides, however, the ability of examining in detail the contribution and interaction of each nonlinear current and has therefore been used in this work to provide a good insight to the HBT distortion mechanisms.

Manuscript received March 31, 1992; revised July 28, 1992. This work has been supported by Alcatel-Espace (Contract No. 393/550 760), Bell Northern Research and ARO (Contract No. DAAL03-92-G-0109).

The authors are with the Center for High Frequency Microelectronics, Solid State Electronics Laboratory, Department of Electrical Engineering and Computer Science, The University of Michigan, Ann Arbor, MI 48109-2122.

IEEE Log Number 9203713.

The good IMD3 performance of HBT's has been attributed to partial cancellation of the IM currents generated by the emitter resistive and capacitive elements [7], [8]. Using a very simple model with only two nonlinearities (the base-emitter conductance and the base-emitter junction capacitance) Maas [8] has, for example, proven this mechanism under certain assumptions. In reality, however, only partial IM current cancellation occurs due to the rather small capacitive nonlinearity as evidenced by the increase of the third (or second) order intercept point, IP3 (IP2) with frequency [8].

A first analysis of the HBT nonlinear characteristics by considering all the device nonlinearities was recently presented by the authors [9], using a hybrid-π model and a Volterra Series approach. It was found that absence of C_{je}, g_{je} and g_m would degrade IMD3 while the opposite occurs for the C_{bc} generated current. Interactions between these elements were found to define the final IMD3 performance. This paper provides further insight into the HBT distortion characteristics through the help of a more physical model based on the T rather than π configuration. The modeling technique used was based on Volterra Series and is described in Section II. Section III describes the experimental characterization procedure and results. The analysis of the various nonlinear currents and the way they interact to determine the IMD3 characteristics are finally described in Section IV. Details on the effect of second harmonic load termination on distortion are also presented in the same section.

II. Distortion Modeling by Volterra Series

The large signal equivalent circuit model used for the HBT analysis is shown in Fig. 1. An intrinsic T configuration is employed together with all the external parasitics. The extraction technique used for the equivalent circuit elements is discussed in Section III. The four major sources of nonlinearity are the base-emitter capacitance, C_{je}, the base-emitter conductance, g_{je}, the base-collector capacitance, C_{bc} and the common gain current gain, α. The small signal currents (or charges) of all nonlinear elements are described in the quasilinear case as

$$i = \frac{\partial f}{\partial V_{be}} v_{be} + \frac{\partial f}{\partial V_{ce}} v_{ce}, \tag{1}$$

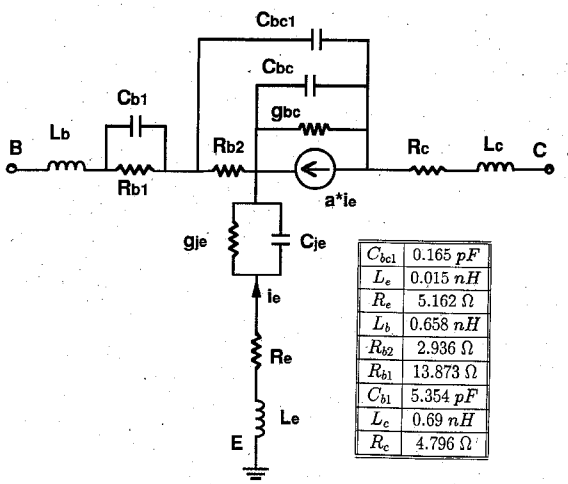

C_{bc1}	0.165 pF
L_e	0.015 nH
R_e	5.162 Ω
L_b	0.658 nH
R_{b2}	2.936 Ω
R_{b1}	13.873 Ω
C_{b1}	5.354 pF
L_c	0.69 nH
R_c	4.796 Ω

Fig. 1. HBT large signal model.

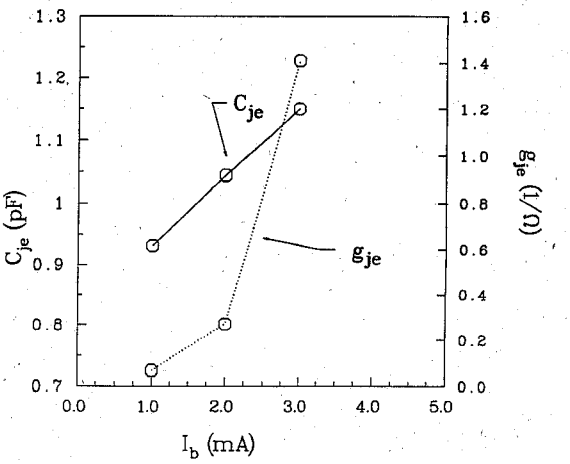

Fig. 2. C_{je} and g_{je} bias dependence of the HBT.

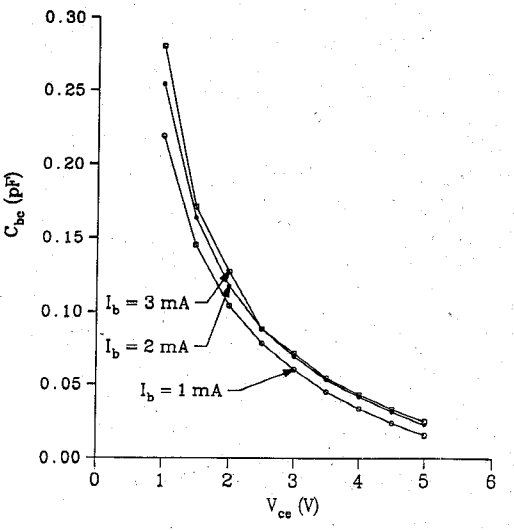

Fig. 3. C_{bc} bias dependence of the HBT.

where f represents the large signal parameter of the particular nonlinearity. All f's are frequency independent except for α due to signal delay considerations. The derivatives $(\partial f/\partial V)$ in (1) represent small signal values and can be obtained experimentally through bias dependent S-parameter measurements.

The C_{je} and g_{je} bias dependencies are shown in Fig. 2. Since both elements depend on V_{be} only, the derivatives with respect to V_{ce} are set to zero and the following expressions were used:

$$C_{je} \equiv \frac{\partial f_{qje}}{\partial V_{be}} \equiv c_0 + c_1 I_b, \tag{2}$$

$$g_{je} \equiv \frac{\partial f_{ije}}{\partial V_{be}} = g_0 + g_1 I_b + g_2 I_b^2. \tag{3}$$

g_1 was forced to be equal or very close to its value obtained through differentiation of the dc base current over V_{be} given by, $I_b = I_s e^{qV_{be}/\eta kT}$.

The above relation was used to convert all I_b dependencies to V_{be} dependencies. This allows one to expand the bias dependencies for C_{je} and g_{je} in a Taylor Series of the voltage, V_{be}. Third order Volterra Series analysis accounts for derivatives of these small-signal elements with respect to V_{be} up to second order. This corresponds to the third order derivatives with respect to V_{be} of the large signal quantities (f_{ije}, f_{qje}) used in equations 1 through 3.

C_{je} consists, in general, of three components: the base(B)-emitter(E) depletion capacitance, the diffusion capacitance and a component due to charge storage at the dip created by the conduction band discontinuity at the base-emitter junction. The contribution of each component to the overall C_{je} value depends on design and operating conditions. In the particular case of the HBT's investigated in this study, C_{je} was small due to small device area and graded E-B heterointerface. Furthermore, the devices showed a weaker dependence of C_{je} than g_{je} on I_b compared to g_{je}. This implied a smaller contribution of C_{je} than g_{je} to the device nonlinearity. Although this is true for the investigated devices, the situation may be different for other HBT designs and different operating conditions.

The base-collector(C) capacitance bias dependence is shown in Fig. 3. C_{bc} is primarily V_{ce} dependent and its bias dependence can be found by fitting the measured data to the expression,

$$C_{bc} \equiv \frac{\partial f_{qbc}}{\partial V_{bc}} = \frac{1}{\sqrt{c_{b0} + c_{b1} V_{ce} + c_{b2} V_{ce}^2 + \cdots}}. \tag{4}$$

The compatibility of C_{bc} with equation 1 was ensured by considering $v_{bc} = v_{be} - v_{ce}$ and since,

$$q_{bc} = \frac{\partial f_{qbc}}{\partial V_{be}} v_{be} + \frac{\partial f_{qbc}}{\partial V_{ce}} v_{ce}, \tag{5}$$

we obtain

$$\frac{\partial f_{qbc}}{\partial V_{be}} = \frac{\partial f_{qbc}}{\partial V_{bc}} \equiv C_{bc} \tag{6}$$

and

$$\frac{\partial f_{qbc}}{\partial V_{ce}} = -\frac{\partial f_{qbc}}{\partial V_{bc}} \equiv -C_{bc}. \tag{7}$$

The small signal current through α is given by

$$i_a = \frac{\partial I_c}{\partial I_e} i_e \equiv \alpha i_e. \tag{8}$$

Since $i_e = -(g_{je} + j\omega C_{je})v_{be}$, this relation becomes

$$i_a = -\alpha(g_{je} + j\omega C_{je})v_{be} \equiv \frac{\partial f_{iga}}{\partial V_{be}} v_{be}, \tag{9}$$

where,

$$\alpha = \alpha_0 \frac{e^{-j\omega\tau}}{1 + j\dfrac{\omega}{\omega_a}}. \tag{10}$$

The bias dependencies of α_0 and $f_a \equiv \omega_a/2\pi$ are shown in Fig. 4 while τ versus V_{ce} is shown in Fig. 5. All these parameters depend only on V_{be}, except τ which depends only on V_{ce}. Furthermore, all derivatives of the large signal current, f_{iga}, flowing through α with respect to V_{ce} are zero. The I_b dependence of α_0 and f_a were considered by

$$\alpha_0 = a_{00} + a_{01}I_b \tag{11}$$

and

$$f_a = f_0 + f_1 I_b. \tag{12}$$

Finally, the V_{ce} dependence of the transit time τ is given by

$$\tau = \sqrt{t_0 + t_1 V_{ce} + t_2 V_{ce}^3}. \tag{13}$$

The probing method [10]–[12] was used to implement the Volterra Series theory and the analysis of the IMD3 mechanisms was made up to third order approximation. The input signal exciting the HBT can be described using Volterra Series as follows:

$$v_s(t) = \sum_{i=1}^{K} A_i e^{j\omega_i t}. \tag{14}$$

If $v_j(t)$ is the voltage at node j, then this voltage can be expressed, to an nth order approximation, in terms of the mth order nonlinear transfer functions, $H_{jm}(j\omega_1, j\omega_2, \cdots, j\omega_m)$ (with $m = 1, 2, 3, \cdots, n$), as follows:

$$v_j(t) = \sum_{m=1}^{n} v_{jm}(t), \tag{15}$$

where

$$v_{jm}(t) = \sum_{k_1=1}^{K} \sum_{k_2=1}^{K} \cdots \sum_{k_m=1}^{K} \left(\prod_{i=1}^{m} A_{k_i} \right) \cdot H_{jm}(j\omega_{k_1}, j\omega_{k_2}, \cdots, j\omega_{k_m}) \cdot \exp\left(j\omega_{k_1}t + j\omega_{k_2}t + \cdots + j\omega_{k_m}\right)t. \tag{16}$$

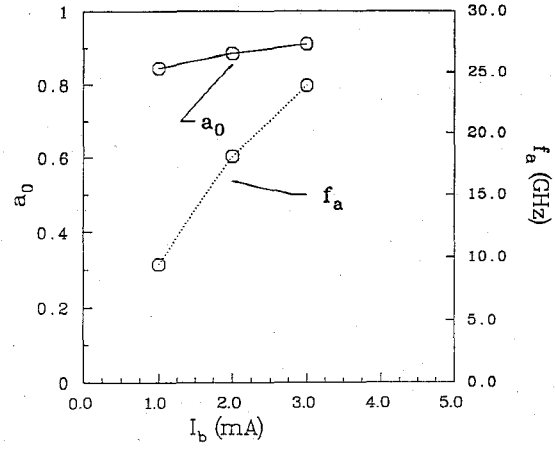

Fig. 4. a_0 and f_a bias dependence of the HBT.

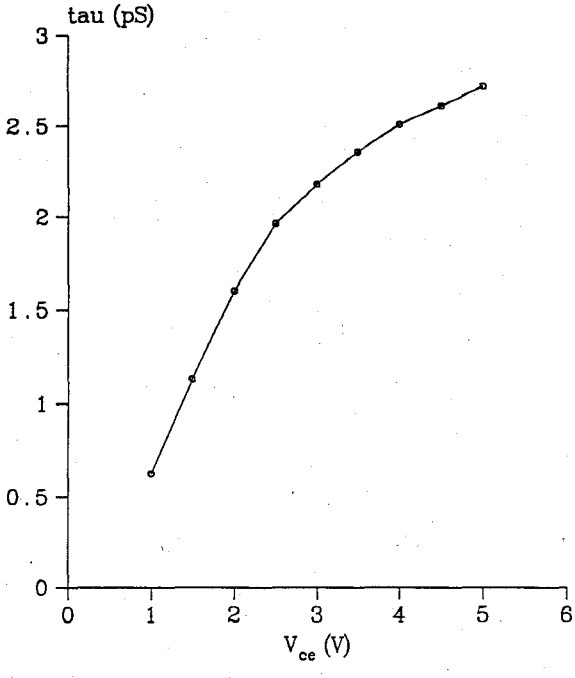

Fig. 5. τ bias dependence of the HBT.

The calculation of the nonlinear transfer functions is performed sequentially, from lowest to highest order, by solving linear systems of equations. The first order transfer functions determine the response of the linear circuit, while the second or higher order functions account for the device's nonlinear behavior. Nonlinear currents were defined for second or higher order calculations. The second (or third) order nonlinear transfer functions are calculated by solving the linear system corresponding to nonlinear currents of the respective order.

Given a real source voltage, the fundamental and third order intermodulation voltage at frequency $2\omega_1 - \omega_2$ for node k and to a third order accuracy are given by

$$v_{k,\omega_1}(t) = \tfrac{1}{2} B_k e_2^{j\omega_1 t} + \tfrac{1}{2} B^* e^{-j\omega_1 t} \tag{17}$$

$$v_{k,2\omega_1-\omega_2}(t) = \tfrac{1}{2} C_k e^{j2\omega_1 t - j\omega_2 t} + \tfrac{1}{2} C_k^* e^{-j2\omega_1 t + j\omega_2 t} \tag{18}$$

where

$$B_k = A_1 H_{k1}(j\omega_1) + \tfrac{3}{4}|A_1^2| A_1 H_{k3}(-j\omega_1, j\omega_1, j\omega_1) + \tfrac{3}{2}|A_2^2| A_1 H_{k3}(-j\omega_2, j\omega_1, j\omega_2) \quad (19)$$

and

$$C_k = \tfrac{3}{4} A_1^2 A_2^* H_{k3}(j\omega_1, j\omega_1, -j\omega_2). \quad (20)$$

Consequently, the power absorbed by the load at the fundamental frequency, ω_1, is given by,

$$P_{\text{out}} = \tfrac{1}{2}|B_4|^2 |Y_l(j\omega_1)| \cos[\angle Y_l(j\omega_1)]. \quad (21)$$

Similarly, the power absorbed by the load at the frequency $2\omega_1 - \omega_2$ is the third order intermodulation product (IMD3), given by

$$P_{\text{IMD3}} = \tfrac{1}{2}|C_4|^2 |Y_l(j2\omega_1 - j\omega_2)| \cdot \cos[\angle Y_l(j2\omega_1 - j\omega_2). \quad (22)$$

Finally, the input power is given by,

$$P_{\text{in}} = \tfrac{1}{2}|B_1|^2 |Y_{\text{in}}(j\omega_1)| \cos[\angle Y_{\text{in}}(j\omega_1), \quad (23)$$

where Y_{in} is the transistor input admittance seen from port 1.

III. Experimental Characterization and Modeling Procedure

The devices characterized were AlGaAs/GaAs HBT's with total emitter area of 200 μm^2. Load Pull measurements were performed under single and double tone excitation with signals at frequencies $f_1 = 8$ GHz and $f_2 = f_1 + \Delta f$, where $\Delta f = 100$ kHz. An automated tuner system by *Focus Microwaves Inc.* was used for this purpose. DC bias was selected for Class-AB operation. The source impedance was set close to its simultaneous match value to assure maximum gain. The T-model, shown in Fig. 1, was used for device simulations.

Multibias S-parameter tests at different I_b's and V_{ce}'s and equivalent circuit extractions at each one of them permitted the evaluation of the base current (I_B) and collector-emitter voltage (V_{CE}) dependence of all circuit parameters considered to be nonlinear (i.e., C_{je}, g_{je}, C_{bc} and α). This was carried out by fitting the equivalent circuit parameters of the HBT to the measured S-parameters at a bias point which coincided with the bias condition used for the intermodulation experiments and analysis; Class-AB operation in the case of the HBT studies reported here. Once all model elements were evaluated at this bias point, the linear elements (e.g., R_e, L_e, L_c, R_c etc.) were kept constant for the remaining (different bias) S-parameter fittings, and the only variables were the nonlinear equivalent circuit parameters. C_{je}, g_{je}, α_0 and f_a were considered as I_b only dependent elements. Similarly, τ was considered to depend only on V_{ce}. All S-parameters were measured over the frequency range of 1.5 to 26.5 GHz using a HP 8510B Network Analyzer. I_b versus V_{be} tests (Gummel plots) were used to convert from I_b to V_{be} dependence. The IMD3 products were measured using a TEKTRONIX spectrum analyzer. Typical bias dependencies of the various equivalent circuit elements are shown in Table I.

TABLE I
Parameters for the Elements Bias Dependencies

Parameter	Value
c_0	0.821555 pF
c_1	0.109497 pF/mA
g_0	−2.0087 S
g_1	1.13903 S/mA
c_{b0}	565.573 1/pF^2
c_{b1}	−1080.02 1/(V · pF^2)
c_{b2}	704.8021/(V^2 · pF^2)
a_{00}	0.814742
a_{01}	0.032897 1/mA
f_0	2.66697 GHz
f_1	7.24425 GHz/mA
t_0	−2.24375 pS^2
t_1	2.02489 pS^2/V
t_2	0.06017 pS^2/V^3

Volterra Series was next used to analyze the nonlinear characteristics of the intrinsic device. This was carried out by incorporating the parasitic elements L_b, C_{b1}, R_{b1} in the source load and L_c and R_c in the output load. The analysis performed here considers large-signal nonlinearities with respect to the voltages V_{be} and V_{ce} up to third order. Therefore only load responses at dc, the fundamental harmonic and the second harmonic are accounted for. A 50 Ω termination was considered as the output load at dc and at the second harmonic. The source load was set equal to 50 Ω at dc and equal to its conjugate match condition value at the second harmonic. At the fundamental harmonic (8 GHz) both loads were set equal to their conjugate match value to allow for maximum gain. The selected bias point ($I_b = 2$ mA, $V_{ce} = 2.5$ V) corresponds to Class-AB operation. The IP3 of the device was 23 dB and the discrepancy between the experimentally and theoretically determined values of this parameter was 1 dB.

IV. Analysis of IMD3 Characteristics and Relation to Third Order Nonlinear Currents

Optimum output power and IMD3 performance can be controlled simultaneously by adjusting the effects of the various nonlinearities according to variable external load conditions in order to obtain: (i) conjugately matched conditions at the fundamental frequency for maximum gain and (ii) proper second harmonic termination for low IMD3 product. Both conditions are possible by selecting appropriate load (Y_l) frequency responses so that $Y_l(f_1)$ satisfies best the gain requirement while, $Y_l(2f_1)$ (at the second harmonic frequency) provides low IMD3. It should be noted that the loads at dc and the second harmonic are considered at the plane of the intrinsic device terminals, since the parasitic elements L_c, R_c, C_{b1}, R_{c1} and L_b were, for the purpose of the nonlinear analysis, incorporated into the external loads provided by the microwave tuners. The analysis presented here is performed for various $Y_l(2f_1)$

values corresponding to different load reflection coefficient magnitude ($G_{l,2f,mag}$) and phase ($G_{l,2f,ph}$).

The contribution and impact of the model's nonlinear elements on IMD3, can be determined by examining the third order nonlinear currents generated by each element at frequency $2f_1 - f_2$. This also allows the investigation of possible nonlinear current cancellations which may lead to better intermodulation characteristics.

Third order nonlinear currents are proportional to the third order derivatives of the large signal quantities (i.e., f_{ije} etc.) of the various nonlinear elements with respect to V_{be} or V_{ce}. Fig. 6 and 7 show the third order nonlinear currents generated by the four nonlinearities as a function of the phase of the load reflection coefficient, $G_{l,2f,ph}$ at a magnitude equal to $G_{l,2f,mag} = 0.75$. The choice of source and load terminations for this study was explained at the end of Section III. All currents were evaluated at an input power level of -7.32 dBm. Included in this figure are also the sums of the currents generated by g_{je} and C_{je} (indicated as $g_{je} + C_{je}$), the sum of the currents generated by g_{je}, C_{je}, C_{bc} and α together (indicated as $g_{je} + C_{je} + C_{bc} + \alpha$) and the sum of the currents generated by C_{bc} and α (denoted as $C_{bc} + \alpha$); $g_{je} + C_{je} + C_{bc} + \alpha$ is the total third order nonlinear current entering the input base terminal, while $C_{bc} + \alpha$ is the total current entering the output collector node. As one notices, the nonlinear current generated by g_{je} turns out to be the strongest of all elements followed by the current generated by α. The C_{je} and C_{bc} related nonlinear currents are much lower than that of g_{je} (compare Figs. 6 and 7). As a result, the total B-E and B-C currents, $g_{je} + C_{je}$ and $C_{bc} + \alpha$, respectively, are not much different than the g_{je} and α alone related currents. Also, due to the much lower C_{je} related current no significant B-E nonlinear current cancellation is observed. Total cancellation of the third order currents is, in any case theoretically, impossible according to Maas *et al.* [8]. One, however, must bear in mind that a more pronounced cancellation may be true for the second order currents. Partial current cancellation was observed among the total B-E and B-C currents: the total current entering the base junction ($g_{je} + C_{je} + C_{bc} + \alpha$) is lower by almost a factor of 2 compared to the individual junction currents ($g_{je} + C_{je}$ and $C_{bc} + \alpha$), for all second harmonic output load coefficients.

Fig. 8 shows the corresponding phases of all nonlinear currents discussed above. Nonlinear current cancellation between currents entering a node occurs at the point where the phase difference of the participating elements is greater than $\pi/2$. One notices a difference of $\simeq 210°$ between the $C_{je} + g_{je}$ and $C_{bc} + \alpha$ generated currents. It is also interesting to note that, the difference between the phases of C_{je} and g_{je}, as well as C_{bc} and α currents, is of the order of 90° and 150°, respectively. Cancellation is, however, not noticeable because of the large difference of the individual current magnitudes. Under different bias or frequency conditions g_{je} and C_{je} or C_{bc} and α may, however, show different magnitude and phase relations leading consequently to other cancellation features.

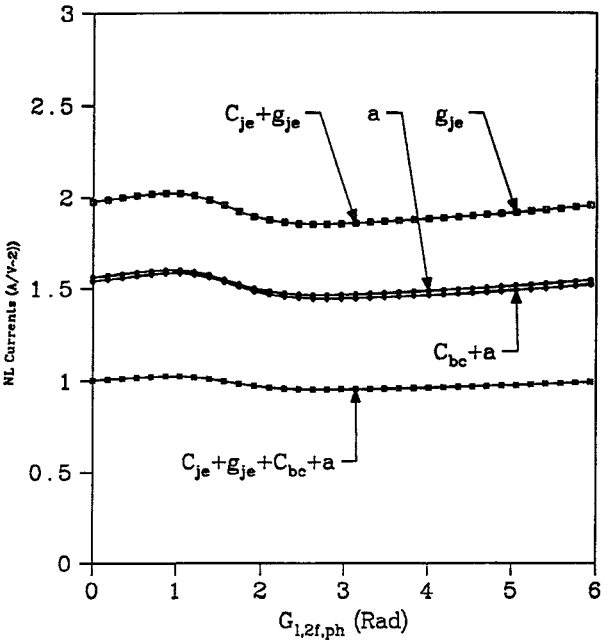

Fig. 6. Third order nonlinear current magnitudes of g_{je} and α versus the Phase, $G_{l,2f,ph}$, of the second harmonic load at $G_{l,2f,mag} = 0.75$.

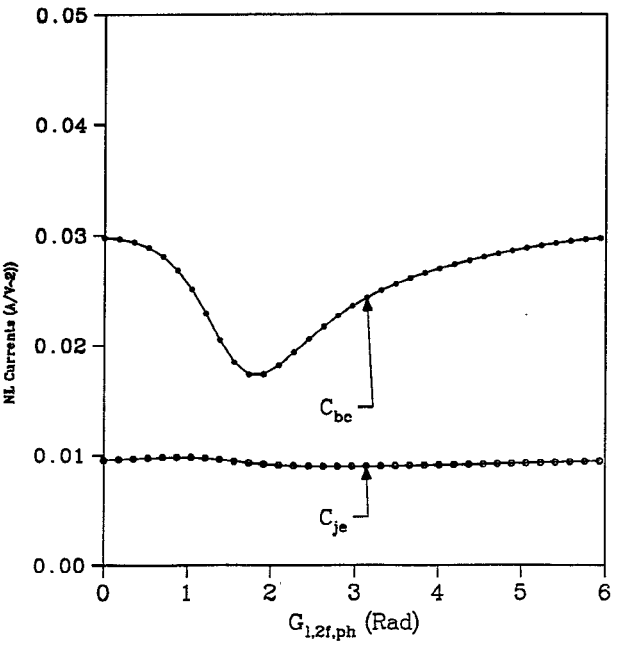

Fig. 7. Third order nonlinear current magnitudes of C_{bc} and C_{je} versus the phase, $G_{l\ 2f,ph}$, of the second harmonic load at $G_{l,2f,mag} = 0.75$.

The contribution of each element and its importance on IMD3 can be evaluated by comparing the IMD3 value when all nonlinearities are present with its value when the third order nonlinear current of a particular element is substantially reduced. This provides a measure of the IMD3 sensitivity on the nonlinear currents and their combinations. Fig. 9 shows IMD3 characteristics under $G_{l,2f,mag} = 0.75$ termination conditions when all elements are present, as well as, when the nonlinear currents due to particular elements or combination of them are eliminated. The sensitivity of IMD3 on a particular element is

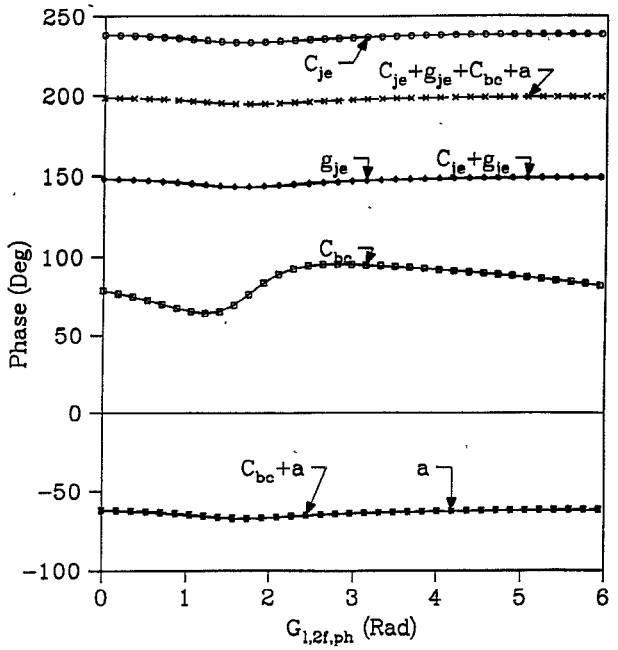

Fig. 8. Third order nonlinear current phases versus the phase, $G_{l,2f,ph}$, of the second harmonic load at $G_{l\,2f,mag} = 0.75$.

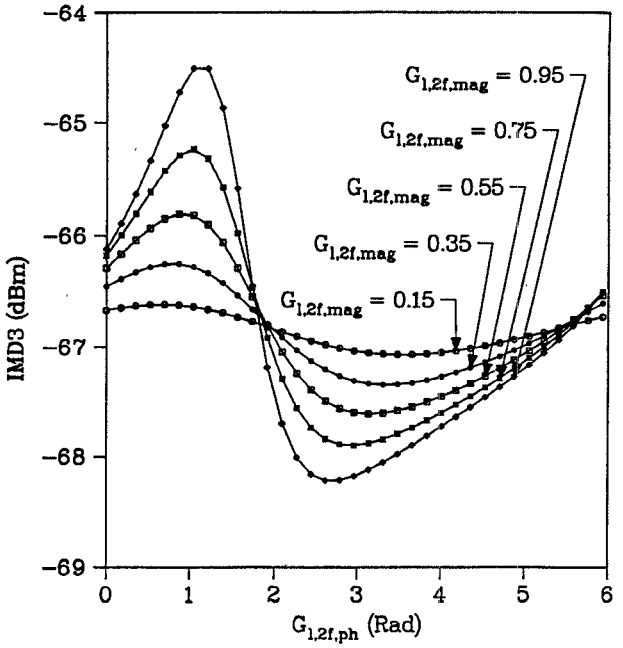

Fig. 10. IMD3 dependence on the phase ($G_{l,2f,ph}$) and magnitude ($G_{l,2f,mag}$) of the second harmonic load.

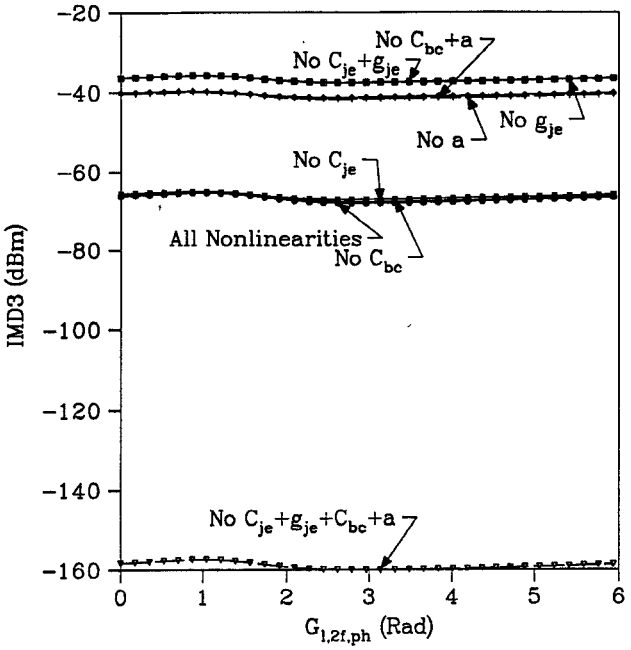

Fig. 9. Sensitivity of IMD3 on third order currents due to various device nonlinearities.

determined not only by its magnitude but also by the position in which it is attached to the circuit. As one notices the sensitivity of IMD3 on the C_{je} or C_{bc} related current is marginal due to their very low magnitudes. IMD3 would degrade if the effect of the α or g_{je} generated third order current is reduced; a factor of 100 reduction was considered in the analysis. The same holds for the $C_{je} + g_{je}$ and the $C_{bc} + \alpha$ related currents. The sensitivity of IMD3 on the latter currents is essentially the same with that observed for g_{je} and α alone due to the dominance of these elements over the other two; this is consistent with the conclusion drawn from Fig. 6 regarding current cancellation. Only when both elements, α and g_{je} or, more generally, $C_{bc} + \alpha$ and $C_{je} + g_{je}$ are present IMD3 can be improved. In this case a partial nonlinear current cancellation occurs (see Fig. 6) resulting in an improved IMD3 level (Fig. 9) over all possible second harmonic output load reflection coefficients. Finally, when all element currents are eliminated (curve labeled "*No* $C_{je} + g_{je} + C_{bc} + \alpha$") IMD3 is largely improved to -160 dB. This result is naturally of theoretical only importance and indicates simply the ultimate degree of distortion that the device could achieve.

The choice of the second harmonic load is important in order to fully optimize the IMD3 characteristics. As one observes in Fig. 6, all nonlinear currents are not constant with second harmonic loads. For phases $G_{l,2f,ph}$ around 1.5 rad the strongest of the elements, g_{je} and α have a maximum while their minimum occurs close to 3 rad. These two regions indicate where the extremes of IMD3 are located as function of $G_{l,2f,ph}$. Fig. 10 shows IMD3 versus $G_{l,2f,ph}$ at an input power of -7.32 dBm for various second harmonic load reflection coefficients, $G_{l,2f,mag}$. Looking at the $G_{l,2f,mag} = 0.75$ curve one sees that a 3 dB variation may occur in IMD3 due to only very small variations of the g_{je} or the α generated currents with $G_{l,2f,ph}$. IMD3 is obviously very sensitive on the dominating nonlinear currents. Furthermore, it is obvious that best IMD3 requires high reflection coefficients having second harmonic phases at the short load impedance region of the Smith chart (around 3 rad).

The lowest and highest IMD3 values are determined, as mentioned above, by the nonlinear current extreme values. Comparison between the results of Figs. 6 and 10

shows that, worst IMD3 occurs at a $G_{l,2f,ph}$ corresponding close to the maximum of the g_{je} or the α related currents. Also, the minima of the IMD3 curves occur in the region where these currents have their minima. In general, best (worst) IMD3 occurs at $G_{l,2f,ph}$ values having high (low) base-emitter ($C_{je} + g_{je}$) or base-collector ($C_{bc} + \alpha$) or total ($C_{je} + g_{je} + C_{bc} + \alpha$) nonlinear current. However, it is the g_{je} nonlinear current that dominates IMD3 generation. The α, $\alpha + C_{bc}$, $C_{je} + g_{je}$ related currents have the same trends with the g_{je} nonlinear current since α reflects the g_{je} characteristics (see equation 9) and the currents of C_{je} and C_{bc} are weak. Overall, it appears that g_{je} is the dominating element in HBT IMD3 performance. The optimum IMD3 evaluated here was found to occur at the same angle where best IMD3 was evaluated using a π-model and a different device as reported earlier on by the authors [9]. The work presented here provides, however, a better insight to the true mechanisms dictating HBT distortion, since the analysis is based on a T-model where each element has more physical significance.

V. Conclusion

The IMD3 performance of HBT's was studied using a generalized Volterra Series approach, which allows device analysis under variable second harmonic load conditions. A T-equivalent circuit model was used for the HBT to provide better physical insight to its nonlinear characteristics. IMD3 was found to be greatly affected by the nonlinear current entering the base junction and for the particular device under study, g_{je} followed by α dominate the nonlinear behavior. Cancellation occurs in the base node through interaction of the g_{je} and α nonlinearities and improves IMD3 performance by at least 15 dB (see Fig. 9). Best IMD3 can be obtained through proper second harmonic load selection and is associated with the minimum of the dominant nonlinear current, namely, g_{je}.

Acknowledgment

The authors would like to thank Doug Teeter, Phil Marsh and Marcel Tutt for providing help during device characterization.

References

[1] M. E. Kim *et al.*, "12–40 GHz low harmonic distortion and phase noise performance of GaAs HBTs," *GaAs IC Symp.* 1988, pp. 117–120.
[2] S. Narayanan, "Transistor distortion analysis using Volterra series representation," *Bell Syst. Tech. J.*, May–June 1967, pp. 991–1024.
[3] S. A. Maas, D. Nelson, "Modeling MESFET's for intermodulation analysis of mixers and amplifiers," *IEEE Trans. Microwave Theory Tech.*, vol. 38, no. 12, pp. 1964–1971, Dec. 1990.
[4] R. A. Minasian, "Intermodulation distortion analysis of MESFET amplifiers using the Volterra series representation," *IEEE Trans. Microwave Theory Tech.*, vol. MTT-28, no. 1, pp. 1–8, Jan. 1980.
[5] G. M. Lambrianou and C. S. Aitchison, "Optimization of third-order intermodulation product and output power from an *X*-band MESFET amplifier using Volterra series analysis," *IEEE Trans. Microwave Theory Tech.*, vol. MTT-33, no. 12, pp. 1395–1403, Dec. 1985.
[6] J. A. Higgins, R. L. Kuvas, "Analysis and improvement of intermodulation distortion in GaAs power FETs," *IEEE Trans. Microwave Theory Tech.*, vol. MTT-28, no. 1, pp. 9–17, Jan. 1980.
[7] S. A. Maas, B. Nelson, and D. Tait, "Intermodulation in heterojunction bipolar transistors," in *1991 IEEE MTT-S Microwave Symp. Dig.*, pp. 91–93.
[8] —, "Intermodulation in heterostructure bipolar transistors," *Trans. Microwave Theory Tech.*, vol. 40, no. 3, pp. 442–448, Mar. 1992.
[9] A. Samelis and D. Pavlidis, "Analysis and optimization of third order intermodulation distortion mechanisms in AlGaAs/GaAs heterostructure bipolar transistors," in *IEEE MTT-S Int. Microwave Symp. Dig.*, Albuquerque, June 1992, pp. 1587–1590.
[10] J. J. Bussgang, L. Ehrman, and J. W. Graham, "Analysis of nonlinear systems with multiple inputs," *Proc. IEEE*, vol. 62, no. 8, pp. 1088–1119, Aug. 1974.
[11] E. Bedrosian and S. O. Rice, "The output properties of Volterra systems (nonlinear systems with memory) driven by harmonic and Gaussian inputs," *Proc. IEEE*, vol. 59, no. 12, pp. 1688–1707, Dec. 1971.
[12] T. T. Ha, *Solid-State Microwave Amplifier Design*. New York: Wiley, 1981, p. 202–282.

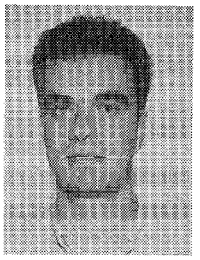

Apostolos Samelis was born in Kalamata, Greece, in 1967. He received the Diploma and Master's degrees, both in Electrical Engineering, from the University of Patras, Greece (1990) and the University of Michigan (1991) respectively. Since 1990 he has been with the University of Michigan as Research Assistant studying towards the Ph.D. degree. His current research interests include nonlinear distortion modeling of HBT's, Monte Carlo simulation and processing of HBT's.

Dimitris Pavlidis (S'73–M'76–SM'83), for a photograph and biography, see this issue, p. 2373.